Biochemical and Biophysical Research Communications 461 (2015) 396–400

Contents lists available at ScienceDirect

Biochemical and Biophysical Research Communications

journal homepage: www.elsevier.com/locate/ybbrc

The NMR solution structure of AIM2 PYD domain from *Mus musculus* reveals a distinct α2–α3 helix conformation from its human homologues

Xianhui Hou [a, b], Xiaogang Niu [a, b, *]

[a] Beijing Nuclear Magnetic Resonance Center, Peking University, Beijing, China
[b] College of Chemistry and Molecular Engineering, Peking University, Beijing, China

ARTICLE INFO

Article history:
Received 20 March 2015
Available online 16 April 2015

Keywords:
Inflammasome
AIM2
PYD
NMR
Solution structure
Self-association

ABSTRACT

The inflammasome is a key component of the innate immune system providing the initial defense against invading organisms. Failure of inflammasome formation is the main reason for many innate and acquired immune diseases. Cytosolic protein absent in melanoma 2 (AIM2) has been reported to play an essential role in double-stranded DNA (dsDNA) sensing and inflammasome formation in response to viruses or bacteria infection. The N-terminal pyrin domain (PYD) of AIM2 interacts with the ASC PYD domain, and then recruits downstream proteins to assemble the AIM2 inflammasome. The molecular mechanisms of PYD mediated signaling remain elusive as limited structural information on PYD family. Herein, we characterized the solution structure of mouse AIM2 PYD domain by NMR spectroscopy, and compared it with the crystal structures of its two human homologues. The comparison shows mAIM2 PYD adopts a unique α2–α3 helix conformation distinct from its human homologues, but similar to the pyrin domain of human NLRP10/PYNOD, which belongs to another family. In addition, the aggregation of mAIM2 PYD domain, with the increased salt concentration, reveals that both the charge surface and hydrophobic interaction play important roles in the self-association of mAIM2 PYD.

1. Introduction

Inflammasomes are signaling platforms which sense a diverse range of microbial products and also a number of stress and damage associated endogenous signals. Inflammasomes are typically composed of an upstream sensor/receptor molecule, an adapter protein known as ASC (apoptosis-associated speck-like protein containing a caspase-activation and recruitment domain (CARD)), and an effector molecule caspase-1 (and/or caspase-11). Upon formation, inflammasomes trigger proteolysis of caspase-1, which subsequently leads to a potent inflammatory response through the maturation and secretion of IL-1 family cytokines, and can then be accompanied by an inflammatory cell death termed pyroptosis [1–3].

Based on the distinct domain architecture, molecule sensors of inflammasomes can be grouped into two families: NOD-like receptors (NLRs) and absent in melanoma 2 (AIM2)-like receptors (ALRs). Most NLRs contain an N-terminal interaction domain (PYD, CARD, or BIR) that interacts with downstream signaling molecules to trigger and regulate inflammatory responses [3], followed by a nucleotide-binding and oligomerization domain (NACHT or NBD), and a C-terminal leucine-rich repeat (LRR) responsible for autoinhibition [4]. ALRs, including AIM2 and interferon-inducible protein 16, can form an inflammasome scaffold without the oligomerization domain in NLRs by clustering upon multiple binding sites in the ligand, dsDNA. AIM2 mainly locates in the cytoplasm of a cell, with a PYD domain at the N terminal and an HIN domain at the C terminal. When the dsDNA from microbes—such as DNA viruses and bacteria—enter the cytoplasm, the HIN domain of AIM2 will recognize and bind to dsDNA, and the PYD domain will bind to the PYD domain of the ASC protein inducing the inflammasome formation and the following immune response [5–7]. AIM2 has been documented to be an important factor in the immune responses against DNA viruses and bacteria, such as the vaccinia virus, mouse cytomegalovirus, *Francisella tularensis* and *Listeria monocytogenes*, as well as a significant role in autoimmune disorders such as psoriasis [8–13].

* Corresponding author. Beijing Nuclear Magnetic Resonance Center, Peking University, Beijing 100871, China. Fax: +86 10 6275 3790.
E-mail address: niuxg@pku.edu.cn (X. Niu).

http://dx.doi.org/10.1016/j.bbrc.2015.04.046
0006-291X/

PYD belongs to the death domain (DD) superfamily, which also includes two other subfamilies—CARD and death effector domain (DED) [14]. Many PYDs oligomerize and interact with other PYD-containing proteins to assemble oligomeric multiprotein signaling complexes, such as inflammasomes [3]. The molecular mechanisms of PYD-mediated signaling events are not clearly, mainly because of the lack of structural information on PYD–PYD complexes.

PYD domains tend to aggregate at high concentrations. Two crystal structures of the human AIM2 (hAIM2) PYD domain have been reported and overcome the aggregation problem by fusing it with a large maltose binding protein (MBP) tag or making a F27G mutant [15,16]. Here, we present the solution structure of wild type (WT) mouse AIM2 (mAIM2) PYD domain with just an N-terminal His tag. Although the mAIM2 PYD shares a highly similar amino acid sequence with hAIM2 PYD of 56% sequence identity, the solution structure of mAIM2 PYD shows a unique α2–α3 helix conformation distinct from those two crystal structures; and this unique conformation may be related to its functional interaction with ASC.

2. Materials and methods

2.1. Construct design, protein expression and purification

The DNA fragment encoding *Mus musculus* $AIM2^{PYD}$ (residues 1–95) was cloned into the pET28a(+) vector (Novagen) with N-terminal His_6-tag, and expressed in *E. coli* Rosetta (DE3) strain (Novagen) with 0.4 mM isopropyl β-D-1-thiogalactoside (IPTG) induction when OD600 reached 1.0, followed by 8hr incubation at 37 °C. Protein was purified with Ni-NTA Sepharose (QIAGEN) under denaturing condition, followed by renaturing through diluting rapidly into an ice-cold buffer (45 mM citric acid, 50 mM Na_2HPO_4, 10% (v/v) glycerol, at pH 3.7). For the preparation of the NMR samples, M9 minimal media and isotopes (^{13}C-glucose and $^{15}NH_4Cl$) were used during the cell culture. All NMR samples were prepared in 20 mM HAc/NaAc buffer (pH 4.0) with 0.01% NaN_3 including 90% H_2O/10% D_2O.

2.2. NMR spectroscopy and structure determination

All NMR spectra were acquired at 25 °C on Bruker 700 MHz and 600 MHz NMR spectrometer both equipped with cryo-probes. The $^{15}N/^{13}C$-labeled AIM2 PYD domain protein samples were prepared in NMR buffer to a final sample volume of 450 μl and a final concentration of about 0.5 mM. The 2D and 3D NMR experiments including $^{1}H–^{15}N$ HSQC, HNCO, HNCACB, CBCA(CO)NH, TOCSY-HSQC, CC(CO)NH, HC(CO)NH, (H)CCH-TOCSY, and HCCH–COSY were utilized for backbone and side chain resonances assignments [17]. NOE distance restraints were obtained from ^{15}N-edited NOESY-HSQC and ^{13}C-edited NOESY-HSQC spectra (120 ms mixing time). All NMR data were processed with the software NMRPipe [18] and analyzed by the software CcpNmr Analysis [19].

Structure calculation used the distance restraints from $^{15}N–$ and ^{13}C-edited NOESY spectra, and the dihedral angle restraints generated by TALOS + based on chemical shifts of the backbone ^{1}H, ^{15}N, C_α, $C_\beta$and CO atoms [20]. The highly flexible N-terminal His_6-tag was excluded in the structure calculation because there was almost no cross peaks of this part observed in the NOESY spectra. The initial structure was calculated by Cyana 2.1 [21] and further refined by CNS 1.3 [22]. One hundred structures were calculated in this process, and an ensemble of the 20 best structures with the lowest energy was obtained. The final structures were analyzed with PROCHECK [23] and visualized using MOLMOL [24].

The 1D ^{1}H spectra of unlabeled mAIM2 PYD with water suppression were acquired on Bruker 700 MHz spectrometer at a concentration of about 0.1 mM. After first measurement of mAIM2 PYD in 20 mM HAc/NaAc, pH4.0 buffer, 20 μl of 2M NaCl stock was added to the 400 μl sample, which made the NaCl concentration to 100 mM. The first 1D ^{1}H spectrum was recorded immediately, and the final one measured after 20 h. Spectra were processed with Bruker® TopSpin® 3.2.

3. Results and discussion

3.1. Solution structure of mAIM2 PYD

The structure of mAIM2 PYD was determined using 1388 experimental NMR restraints, including 1264 NOE-derived distance restraints and 124 dihedral angle restraints. A summary of the structural statistics for these 20 structures is given in Table 1. Analysis of a Ramachandran plot for the ensemble of 20 structures indicates that all the residues are in the allowed region. The averaged root-mean-square deviation (RMSD) value of the 20 structures to the average structure was 0.84 ± 0.03 Å for the heavy atoms of residues from 1 to 92 (Fig. 1A). The atomic coordinates and NMR-derived restraints of mAIM2 PYD have been deposited in the PDB with accession code 2n00. The structure adopts a six-helix bundle which is conserved in the DD fold superfamily (Fig. 1B).

3.2. Structure comparison between mAIM2 PYD and hAIM2 PYD domains

The secondary structure distribution is very similar to the solution structure of mAIM2 PYD and the crystal structure of its two human homologues [15,16]. The overall RMSD of the mAIM2 PYD solution structure to crystal structure of WT hAIM2 PYD is 1.9 Å and 2.0 Å to the crystal structure of F27G hAIM2 PYD. Superimposed with these two crystal structures, the significant local structural difference was observed at the α2–α3 helix (Fig. 2B). Interestingly, it is also the main difference between the two crystal structures of hAIM2 PYD. In the solution structure of mAIM2 PYD, as shown in Fig. 2C, the α3 helix is close to the N terminal of the α2 helix, while the α3 helix is close to the C terminal of α2 helix in the crystal structure of F27G hAIM2 PYD, while the α3 helix of the crystal structure of WT hAIM2 PYD is located in between of the above two.

Structure comparison shows that the solution structure of mAIM2 PYD adopts a unique conformation of α2–α3 helices distinct from its human homologues. Is this conformation special in the PYD family? We looked through other PYD domains, and found that the α3 helix of the PYD domain in human NLRP10 is also close to the N terminal of its α2 helix [25].

Table 1
Structural statistics for the final 20 simulated annealing structures of mAIM2 PYD.

	mAIM2 PYD domain
NOE distance restraints	
All	1264
Short range (|i-j| ≦ 1)	692
Medium range (1 <|i-j|< 5)	369
Long range (|i-j| ≧ 5)	203
Dihedral restraints	124
Averaged RMSD from the average coordinate (Å)[a]	
Backbone atoms (N, C_α, C_β,C′, O)	0.40 ± 0.05 Å
Heavy atoms	0.84 ± 0.03 Å
Ramachandran plot (%)	
Residues in most favored regions	92.3
Residues in additional allowed regions	7.7
Residues in generously allowed regions	
Residues in disallowed regions	

[a] Calculation of RMSD used residues 1–92.

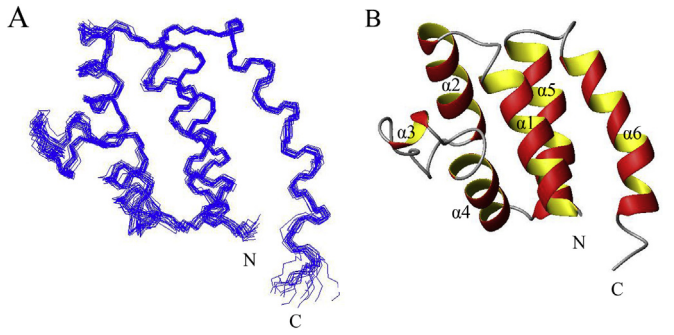

Fig. 1. Three-dimensional structure of mAIM2 PYD determined by NMR spectroscopy. (A) Superposition of the backbone atoms of the 20 final solution structures of mAIM2 PYD. (B) Ribbon representation of the tertiary structure of mAIM2 PYD. The secondary structure elements, six α helices, are labeled.

NLRP10 (also named as PYNOD), which lacks the ligand-binding leucine-rich repeat, is a unique member of the NLRP subfamily. Human NLRP10 interacts with ASC through PYD domain and suppresses the aggregation of ASC [26,27]. Previous study shows the unique location of α3 helix make the human NLRP10 PYD domain interact with ASC PYD through two surfaces composed either with α2–α3 helices or helix α1, loop α3–α4 and helix α4 [25]. The mouse NLRP10 has no inhibition to ASC aggregation [26], whereas its α2–α3 helices also display a drastic difference from its human homologue [25]. The above results collectively indicate that mNLRP10 may not be the one that plays NLRP10's role in mice. Since mAIM2 PYD adopts similar α2–α3 helix conformation as human NLRP10 PYD, it is a reasonable assumption that mAIM2 PYD may interact with ASC PYD in the same model as human NLRP10 PYD. Further research will be performed to prove this assumption.

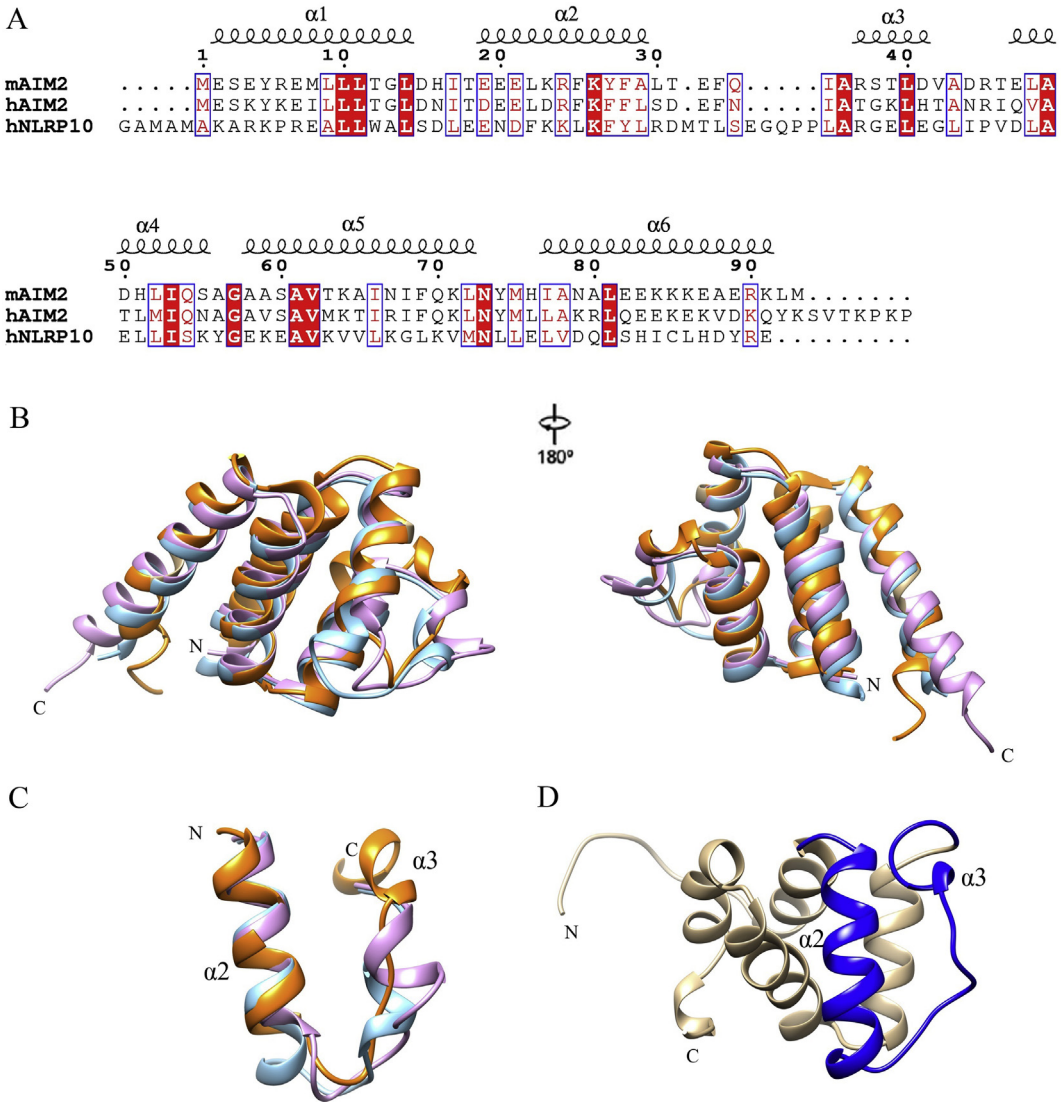

Fig. 2. Comparison of structures of mAIM2 PYD, hAIM2 PYD and hNLRP10. (A) Sequence alignment of mAIM2 PYD, hAIM2 PYD and hNLRP10 with the corresponding secondary structure elements on the top of the sequence. (B) Overlaid solution structure of mAIM2 PYD (orange), F27G hAIM2 PYD (cyan), WT hAIM2 PYD fused with MBP (pink, MBP tag not shown). (C) Overlaid α2-α3 helix part of mAIM2 PYD (orange), F27G hAIM2 PYD (cyan), WT hAIM2 PYD fused with MBP (pink). (D) Solution structure of hNLRP10 PYD with α2-α3 helix part highlighted with blue. All the protein figures are drawn by UCSF Chimera software. (For interpretation of the references to colour in this figure legend, the reader is referred to the web version of this article.)

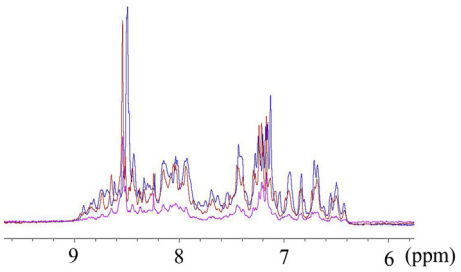

Fig. 3. 1D ^{1}H spectra of amide NH regions of mAIM2 PYD in 20 mM HAc/NaAc, pH 4.0 buffer (blue), with 100 mM NaCl (red), and 20 h after 100 mM NaCl added (pink). (For interpretation of the references to colour in this figure legend, the reader is referred to the web version of this article.)

3.3. Hydrophobic interaction and PYD association

PYD domains tend to form large aggregates and insoluble when expressed alone, which perhaps reflects potential functional PYD–PYD interaction module. To overcome this problem, crystallographic analysis of hAIM2 PYD have to fuse it with a large MBP tag or make a F27G mutant [15,16]. In our research of mAIM2 PYD solution structure, this aggregation problem was solved by refolding protein and measuring NMR data at relatively low pH (pH 4.0) buffer. It was noticed that to keep the PYD monomeric for several days, the salt concentration in NMR buffer must be as low as possible. Thus 20 mM HAc/NaAc at pH 4.0 was used as NMR buffer, and mAIM2 PYD could be stable with a concentration around 0.5 mM in this buffer for more than 3 days at 25 °C to ensure the NMR measurement. To test the effect of salt concentration to the solubility of mAIM2 PYD, 100 mM NaCl was added to the NMR sample. The peak intensity of 1D spectrum was significantly lower with NaCl addition, and after 20 h, the peak intensity was less than 1/4 of that without NaCl (Fig. 3). Since we did not observe significant line broadening of the NMR peaks or protein precipitation, the mAIM2 PYD should be in a mixture state of monomer and aggregation. The aggregated protein could not be observed by NMR spectroscopy because of its large molecular weight, and more protein would shift to aggregated state with time, which made the observed NMR peak intensity get lower continuously. Higher NaCl concentration, such as 200 mM, made mAIM2 PYD aggregate quickly and precipitate.

Recently, it is proposed that AIM2 PYD may self-associate both through charge surface and hydrophobic interaction [16]. Why mAIM2 PYD can maintain monomeric at low pH and low salt concentration is elusive. It may be due to redistribution of surface charge of mAIM2 PYD under pH 4.0 (Fig. 4). At pH 4.0, the surface of mAIM2 PYD should be mainly positive charged, and the repulsive electrostatic force between the positive charged molecules make mAIM2 PYD monomeric in solution. An increase of the NaCl concentration destroyed the protein's surface charge, thereby exposing it to hydrophobic patches on the protein surface and making the protein aggregate through hydrophobic interaction. All the analyses ensure that both charge surface and hydrophobic interaction plays an important role in mAIM2 PYD self-association.

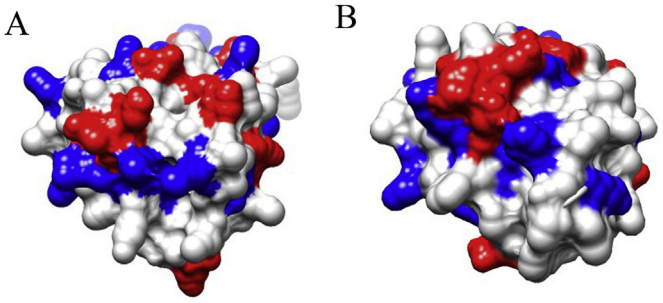

Fig. 4. Surface electrostatic potential of the PYDs of mAIM2 (A) and WT hAIM2 (B) at neutral pH. All surface representations of the PYDs are shown in the same orientation with the α2-α3 helix part in the front. Positive surface charge is colored in blue; negative surface charge is colored red; and neutral surface is in gray. (For interpretation of the references to colour in this figure legend, the reader is referred to the web version of this article.)

Conflict of interest

None.

Acknowledgments

This work was supported by the National Natural Science Foundation of China (31100536). All NMR experiments were performed at the Beijing NMR Center and the NMR facility of National Center for Protein Sciences at Peking University. We would like to thank Dr. Yanli Wang who provided the *AIM2* gene of *Mus musculus*.

Transparency document

Transparency document related to this article can be found online at http://dx.doi.org/10.1016/j.bbrc.2015.04.046.

References

[1] Y. Aachoui, V. Sagulenko, E.A. Miao, K.J. Stacey, Inflammasome-mediated pyroptotic and apoptotic cell death, and defense against infection, Curr. Opin. Microbiol. 16 (2013) 319–326.
[2] T. Strowig, J. Henao-Mejia, E. Elinav, R. Flavell, Inflammasomes in health and disease, Nature 481 (2012) 278–286.
[3] K. Schroder, J. Tschopp, The inflammasomes, Cell 140 (2010) 821–832.
[4] Z. Hu, C. Yan, P. Liu, Z. Huang, R. Ma, C. Zhang, R. Wang, Y. Zhang, F. Martinon, D. Miao, H. Deng, J. Wang, J. Chang, J. Chai, Crystal structure of NLRC4 reveals its autoinhibition mechanism, Science 341 (2013) 172–175.
[5] T. Burckstummer, C. Baumann, S. Bluml, E. Dixit, G. Durnberger, H. Jahn, M. Planyavsky, M. Bilban, J. Colinge, K.L. Bennett, G. Superti-Furga, An orthogonal proteomic-genomic screen identifies AIM2 as a cytoplasmic DNA sensor for the inflammasome, Nat. Immunol. 10 (2009) 266–272.
[6] T. Fernandes-Alnemri, J.W. Yu, P. Datta, J. Wu, E.S. Alnemri, AIM2 activates the inflammasome and cell death in response to cytoplasmic DNA, Nature 458 (2009) 509–513.
[7] V. Hornung, A. Ablasser, M. Charrel-Dennis, F. Bauernfeind, G. Horvath, D.R. Caffrey, E. Latz, K.A. Fitzgerald, AIM2 recognizes cytosolic dsDNA and forms a caspase-1-activating inflammasome with ASC, Nature 458 (2009) 514–518.
[8] Y. Dombrowski, M. Peric, S. Koglin, C. Kammerbauer, C. Goss, D. Anz, M. Simanski, R. Glaser, J. Harder, V. Hornung, R.L. Gallo, T. Ruzicka, R. Besch, J. Schauber, Cytosolic DNA triggers inflammasome activation in keratinocytes in psoriatic lesions, Sci. Transl. Med. 3 (2011), 82ra38.
[9] T. Fernandes-Alnemri, J.W. Yu, C. Juliana, L. Solorzano, S. Kang, J. Wu, P. Datta, M. McCormick, L. Huang, E. McDermott, L. Eisenlohr, C.P. Landel, E.S. Alnemri, The AIM2 inflammasome is critical for innate immunity to Francisella tularensis, Nat. Immunol. 11 (2010) 385–393.
[10] J. Ge, Y.N. Gong, Y. Xu, F. Shao, Preventing bacterial DNA release and absent in melanoma 2 inflammasome activation by a Legionella effector functioning in membrane trafficking, Proc. Natl. Acad. Sci. U.S.A. 109 (2012) 6193–6198.
[11] S. Kim, F. Bauernfeind, A. Ablasser, G. Hartmann, K.A. Fitzgerald, E. Latz, V. Hornung, Listeria monocytogenes is sensed by the NLRP3 and AIM2 inflammasome, Eur. J. Immunol. 40 (2010) 1545–1551.
[12] V.A. Rathinam, Z. Jiang, S.N. Waggoner, S. Sharma, L.E. Cole, L. Waggoner, S.K. Vanaja, B.G. Monks, S. Ganesan, E. Latz, V. Hornung, S.N. Vogel, E. Szomolanyi-Tsuda, K.A. Fitzgerald, The AIM2 inflammasome is essential for host defense against cytosolic bacteria and DNA viruses, Nat. Immunol. 11 (2010) 395–402.
[13] J.D. Sauer, C.E. Witte, J. Zemansky, B. Hanson, P. Lauer, D.A. Portnoy, Listeria monocytogenes triggers AIM2-mediated pyroptosis upon infrequent bacteriolysis in the macrophage cytosol, Cell. Host Microbe 7 (2010) 412–419.
[14] R. Ferrao, H. Wu, Helical assembly in the death domain (DD) superfamily, Curr. Opin. Struct. Biol. 22 (2012) 241–247.
[15] T. Jin, A. Perry, P. Smith, J. Jiang, T.S. Xiao, Structure of the absent in melanoma 2 (AIM2) pyrin domain provides insights into the mechanisms of AIM2

autoinhibition and inflammasome assembly, J. Biol. Chem. 288 (2013) 13225–13235.
[16] A. Lu, V. Kabaleeswaran, T. Fu, V.G. Magupalli, H. Wu, Crystal structure of the F27G AIM2 PYD mutant and similarities of its self-association to DED/DED interactions, J. Mol. Biol. 426 (2014) 1420–1427.
[17] M. Sattler, J. Schleucher, C. Griesinger, Heteronuclear multidimensional NMR experiments for the structure determination of proteins in solution employing pulsed field gradients, Prog. Nucl. Magnetic Reson. Spectrosc. 34 (1999) 93–158.
[18] F. Delaglio, S. Grzesiek, G.W. Vuister, G. Zhu, J. Pfeifer, A. Bax, NMRPipe: a multidimensional spectral processing system based on UNIX pipes, J. Biomol. NMR 6 (1995) 277–293.
[19] W.F. Vranken, W. Boucher, T.J. Stevens, R.H. Fogh, A. Pajon, M. Llinas, E.L. Ulrich, J.L. Markley, J. Ionides, E.D. Laue, The CCPN data model for NMR spectroscopy: development of a software pipeline, Proteins 59 (2005) 687–696.
[20] G. Cornilescu, F. Delaglio, A. Bax, Protein backbone angle restraints from searching a database for chemical shift and sequence homology, J. Biomol. NMR 13 (1999) 289–302.
[21] T. Herrmann, P. Guntert, K. Wuthrich, Protein NMR structure determination with automated NOE assignment using the new software CANDID and the torsion angle dynamics algorithm DYANA, J. Mol. Biol. 319 (2002) 209–227.
[22] A.T. Brunger, P.D. Adams, G.M. Clore, W.L. DeLano, P. Gros, R.W. Grosse-Kunstleve, J.S. Jiang, J. Kuszewski, M. Nilges, N.S. Pannu, R.J. Read, L.M. Rice, T. Simonson, G.L. Warren, Crystallography & NMR system: a new software suite for macromolecular structure determination, Acta Crystallogr. D. Biol. Crystallogr. 54 (1998) 905–921.
[23] R.A. Laskowski, J.A. Rullmannn, M.W. MacArthur, R. Kaptein, J.M. Thornton, AQUA and PROCHECK-NMR: programs for checking the quality of protein structures solved by NMR, J. Biomol. NMR 8 (1996) 477–486.
[24] R. Koradi, M. Billeter, K. Wuthrich, MOLMOL: a program for display and analysis of macromolecular structures, J. Mol. Graph. 14 (1996), 51-&.
[25] M.Y. Su, C.I. Kuo, C.F. Chang, C.I. Chang, Three-dimensional structure of human NLRP10/PYNOD pyrin domain reveals a homotypic interaction site distinct from its mouse homologue, PLoS One 8 (2013) e67843.
[26] R. Imamura, Y. Wang, T. Kinoshita, M. Suzuki, T. Noda, J. Sagara, S. Taniguchi, H. Okamoto, T. Suda, Anti-inflammatory activity of PYNOD and its mechanism in humans and mice, J. Immunol. 184 (2010) 5874–5884.
[27] Y. Wang, M. Hasegawa, R. Imamura, T. Kinoshita, C. Kondo, K. Konaka, T. Suda, PYNOD, a novel Apaf-1/CED4-like protein is an inhibitor of ASC and caspase-1, Int. Immunol. 16 (2004) 777–786.